

Modelling of nanostructured magnetic network media

A. Boboc, I. Z. Rahman (zakia.rahman@ul.ie) and M. A. Rahman*
Materials and Surface Science Institute (MSSI) and Department of Physics,
University of Limerick, National Technological Park, Limerick, Ireland.
* Department of Electronic and Computer Engineering.

Abstract

In this article, we present our results on modelling of patterned magnetic nanonetwork media and on their comparison with available experimental results.

1 INTRODUCTION

Magnetic recording has been going through an exponential growth rate because of the enormous economical potential as ultra high-density information storage media. Nano-fabrication technology has advanced considerably paving the way for production of arrays of identical magnetic nanometer-sized particles or crystallites in the form of dots or wires (also called nano networks) that can be used for information storage. For typical magnetic storage media, the superparamagnetic limit poses a minimum particle size of about 10 nm, that is a maximum recording density of several Tbits / in². This is almost four orders of magnitude higher than the density found in the top-of-the line disk drives today.

With nano-technology, 10 nm size particle can be approached. However, there are many signal-to-noise issues on the way towards reducing the number of particles per bit (more than 10³ at this moment) and reaching the theoretical limit. Inconsistent switching of different particles and an irregular domain structure require averaging over many particles. Simulation of these aspects of nanostructured media is therefore extremely important for the development of usable recording media. Despite the fact that a considerable body of experimental work has been reported on the preparation and properties of the nanostructured magnetic recording materials [1], no significant study has been reported which deals with theoretical models for these structures and their magnetic interaction and recording performance.

2 BACKGROUND

Currently available magnetic recording media consist of continuous thin ferromagnetic films supported by a rigid and nonmagnetic substrate. This type of media shows many tiny polycrystalline grains with a rather broad distribution in size and shape and a random distribution of crystallisation direction. During writing, the write head aligns the otherwise randomly oriented grains into tiny patches. The data is represented by the direction of magnetic moment, area, size and location of this patch. Increasing the areal density of recording media demands

the ability to store a magnetic transition or a bit in the medium at a length as small as possible. It is very well known that the bit length a directly depends on the thickness δ and remanence magnetisation M_r of the material and is inversely proportional to the coercivity H_c of the material as expressed in the following equation:

$$a = \frac{M_r \delta}{2\pi H_c} \quad (1)$$

To increase data storage density, bits to be stored in a given length of the medium require even smaller transition lengths. This leads to a smaller distance between the magnetic reversals and produces strong demagnetising fields on the recorded bit. To enable the stored bit to be stable, the coercive force, H_c , therefore must be high enough to counteract these demagnetising effects.

The remanence and thickness product, $M_r \delta$ must also be small to make the transition length a smaller. At the same time high remanence is required to ensure a sufficient stray magnetic field in the medium, which is required for a sufficient readout signal. To get a high enough remanence, a high saturation magnetisation M_s is required that increases the demagnetising field and necessitates still higher coercivity. The magnetic properties of nanometre sized particles or crystallites differ from the properties of their bulk counterparts as a large fraction of atoms are located on the surface and the interfaces. So the size dependence of magnetisation, anisotropy, Curie transition, coercivity and remnant magnetisation is expected. This poses a physical obstacle to high-density recording in the superparamagnetic limit. For a typical magnetic media this is limited to a minimum particle size of about 10-20 nm. For a grain size below this limit, the orientation of the magnetization changes because of the thermal fluctuations.

The realisation of such small ordered structures is technologically very hard to achieve and expensive to realise when using classical methods such as lithography. Another solution that is also very cheap and easy to implement is the use of the naturally patterned nanostructured media, which are materials that have a very ordered patterned structure.

Porous anodised alumina (commonly known as Nano Channel Alumina, NCA) can be used as a template to fabricate nanostructured materials [1]. Figure 1 shows an example of an ideal patterned media based on NCA

templates where pores are marked with black colour and the white coloured area is the hexagonal structure of the alumina.

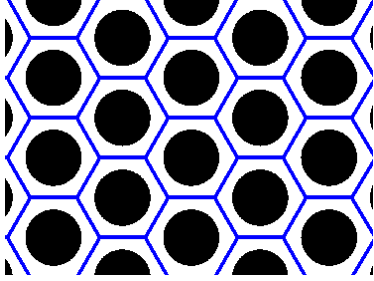


Figure 1: NanoChannel Alumina.

Commercially available NCA templates come with three different pore sizes of nominal diameters of 20, 100 and 200 nm in which nanowires [2] can be grown or the template can be sputtered with magnetic material to form two types of nanonetworks [3]. By controlling various parameters during processing stage of the NCA templates, various pore sizes, inter-pore distances and shapes of patterned nanonetworks can be fabricated [4].

Our study focuses on the theoretical modelling of several magnetic configurations and the comparison of their magnetic behaviour with the experimental values obtained from patterned nanostructured media on NCA.

3 MODELLING OVERVIEW

The equation that describes the dynamics of a magnetic sample in time is the Landau–Lifshitz–Gilbert equation of motion as follows [5]:

$$\frac{d\mathbf{M}}{dt} = -\gamma|\mathbf{M} \times \mathbf{H}_{\text{eff}} + \frac{\alpha}{M_S} \mathbf{M} \times \frac{d\mathbf{M}}{dt} \quad (1a)$$

$$\mathbf{H}_{\text{eff}} = -\frac{1}{\mu_o} \frac{\partial E_{\text{density}}}{\partial \mathbf{M}} \quad (1b)$$

The first term of equation (1a) describes the precession of the magnetization \mathbf{M} about the effective field and the second term describes its dissipation. The constant γ is the gyromagnetic ratio, M_S is the saturation magnetization and \mathbf{H}_{eff} is the effective field that consists of the superposition of the external field and contributions from anisotropy, exchange and demagnetisation fields. The dissipation or magnetic damping is described by the dimensionless constant α called the Gilbert damping parameter.

Solving the Landau-Lifshitz-Gilbert (LLG) equation consists of an algebraic minimization of the total energy E_{total} as follows:

$$E_{\text{total}} = E_{\text{anisotropy}} + E_{\text{exchange}} + E_{\text{demag}} + E_{\text{Zeeman}} \quad (2)$$

The energy terms can be expressed in Cartesian coordinate system as follows:

$$\begin{aligned} E_{\text{exchange}} &= \frac{A}{M_S^2} (|\nabla M_x|^2 + |\nabla M_y|^2 + |\nabla M_z|^2) \\ E_{\text{anisotropy}} &= \frac{K}{M_S^2} (M_x^2 M_y^2 + M_x^2 M_z^2 + M_y^2 M_z^2) \\ E_{\text{demag}} &= \frac{\mu_o}{8\pi} M(r) \cdot \left[\int_V \nabla \cdot \mathbf{M}(r') \frac{\mathbf{r} - \mathbf{r}'}{|\mathbf{r} - \mathbf{r}'|^3} d^2 r' - \int_S \hat{\mathbf{n}} \cdot \mathbf{M}(r') \frac{\mathbf{r} - \mathbf{r}'}{|\mathbf{r} - \mathbf{r}'|^3} d^2 r' \right] \\ E_{\text{Zeeman}} &= \mu_o \mathbf{M} \cdot \mathbf{H}_{\text{ext}} \end{aligned} \quad (3)$$

where, x , y and z are the Cartesian coordinates.

A simple diagram of the implementation of this magnetic modelling is shown in Figure 2. In order to solve the dynamical Landau-Lifshitz-Gilbert equation, the sample geometry, magnetic parameters, the energy distributions and the approximation limits need to be specified.

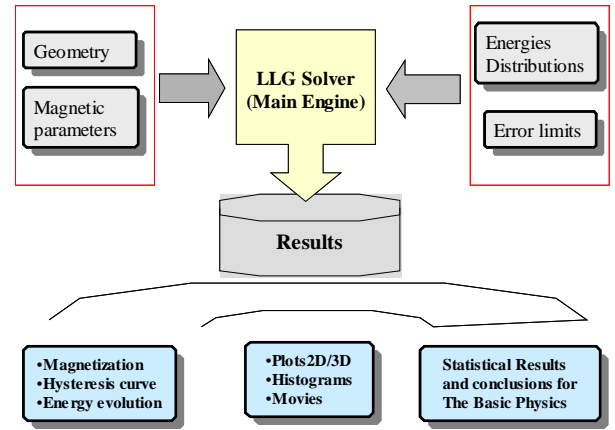


Figure 2: A Simple Diagram of a Magnetic Modelling Algorithm.

The software developed for the present investigation is based on the free available OOMMF (Object Oriented Micromagnetic Framework) codes [6], a public domain micromagnetics program developed at the National Institute of Standards and Technology, USA. The magnetization dynamic equation in time was solved by implementing a first order forward Euler method with step size control on the Landau-Lifshitz ordinary differential equation [7]. Conventional terms for the various contributions to the local field and energy were included in the calculation. The exchange energy was computed via a six neighbour bilinear interpolation described in [8], with Neumann boundary conditions and the magnetostatic energy was calculated using a Fast Fourier Transform based scalar potential. We added modifications to account for nanosize effects such as consideration of the grain size exceeding the superparamagnetic limit and the non uniformity of the surface in determining the magnetization distribution.

4 RESULTS AND DISCUSSION

Two types of patterned nanostructures have been considered, representing different magnetic distributions of the magnetic material as described in Figure 3:

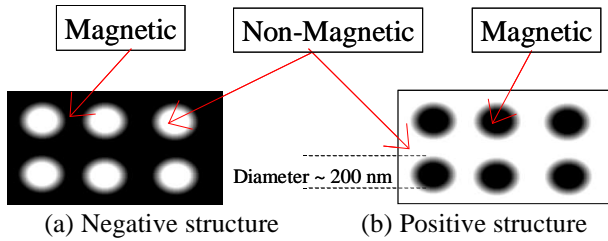


Figure 3: Nanonetwork media.

This simulation work aimed to interpret experimental data that are available in our laboratory. These experimental data are mainly based on iron and nickel based nanostructures deposited by various methods on NCA templates. Therefore, in this paper simulation results are mainly concentrated on the above-mentioned nanostructured samples.

For modelling, wherever possible, the geometry of the pore distribution was defined from non-uniformly distributed pores of the NCA by using the images obtained from SEM analysis of a fabricated sample in our laboratory as shown in Figure 4(a). Figure 4(b) represents the high contrast binary image from a region of the greyscale picture of the SEM patterns [10].

This generated image from the real template provided information about the pore geometry that was used by the code for the generation of magnetic regions.

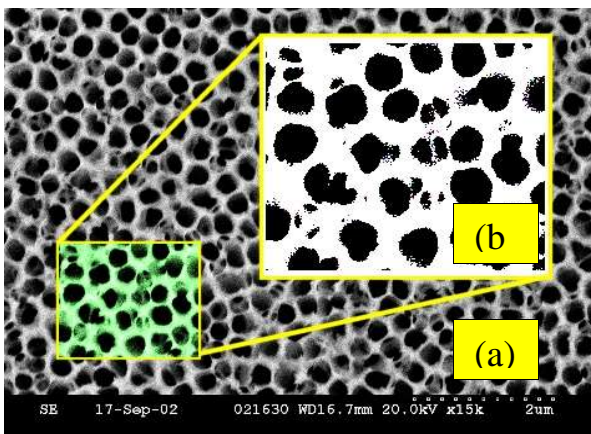


Figure 4: Nickel nanowires grown using electrodeposition method inside pores of NCA templates: (a) SEM image of the Ni wires and (b) High contrast image in B/W of SEM image.

The various studies and analyses that are presented here in order to understand the magnetic properties of the nanopatterned magnetic networks include:

- *Magnetic coercivity behaviour of nanonetworks as a function of applied magnetic field, material composition and sample thickness.*
- *Magnetic properties of the nickel nanowires as a function of NCA pore sizes.*
- *Effects of filling of the pores by magnetic material in the negative nanonetworks.*

4.1 Magnetic coercivity behaviour of nanonetworks as a function of applied magnetic field, material composition and sample thickness

Coercivity values were derived from the model for *cobalt-based negative nanostructures* with a template of 20 nm nominal pore size and for various sample thicknesses. A simulated external field was applied along the nanostructure surface to obtain the hysteresis curves that are shown in Figure 5:

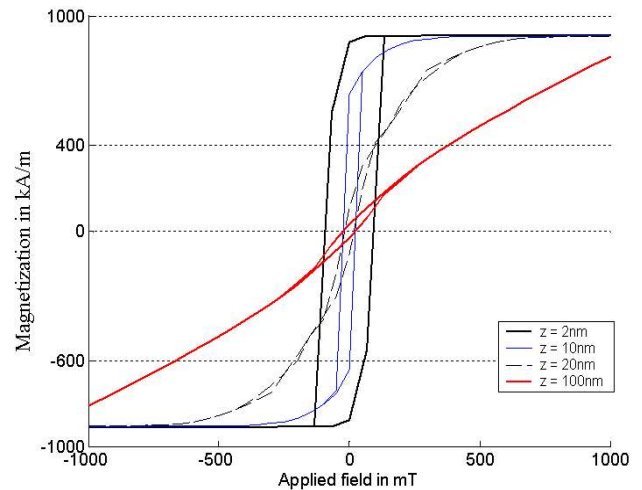


Figure 5: Hysteresis curve dependence on the thickness of Co-based negative nanonetworks.

As can be noticed, for a low thickness (e.g., 2 nm), the magnetic remanence and coercivity are very high. This is good in the sense that a recorded material remains in this state for a long time but a higher field is required for reversing the magnetisation direction. A high coercivity (~ 100 mT) allows the bit size to be small (see Eqn. 1).

For the range 10-20 nm, the media have coercivity curves that have the same shapes that are typical for recording materials [9] with high remanence magnetisation. For higher thickness (e.g., 100 nm) the coercivity remains relatively unchanged but the remanence magnetisation is decreased sharply.

For comparison, the simulation of *iron-based negative nanostructures* is shown in Figure 6. The set-up for simulations was similar to those for Co-based nanonetworks but here only 200 nm pore size samples

were used because experimental data from this type of nanonetwork were available from our laboratory. Coercivity calculations were done for several thickness and the results were compared with the experimental values [1]. Figure 6 shows the dependence of coercivity on the thickness of the nanostructure. A very good agreement may be noticed considering that the simulations were performed on an ideal geometry of the nanonetwork.

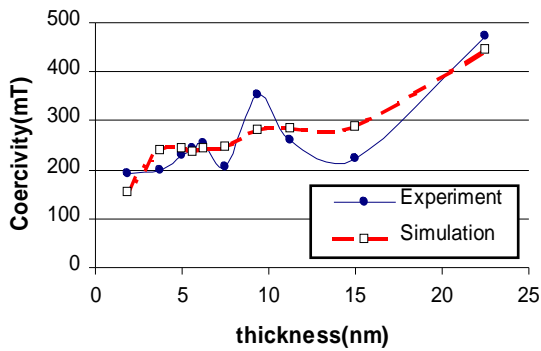
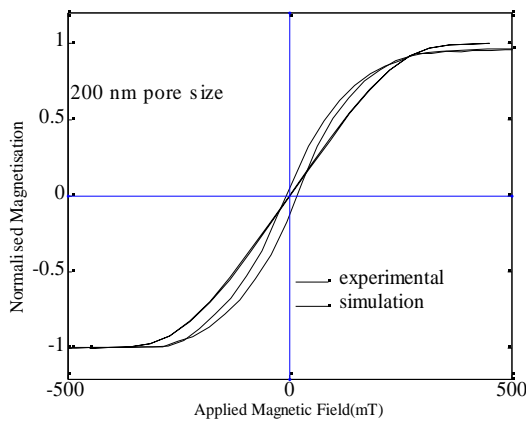
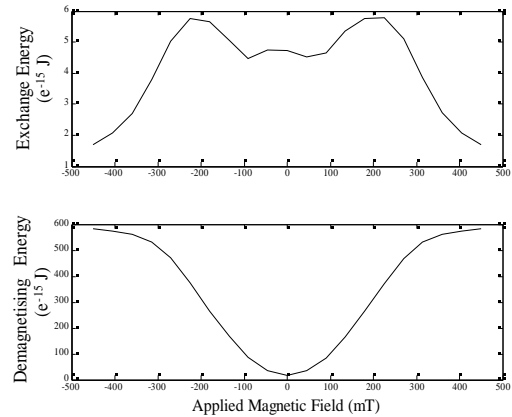


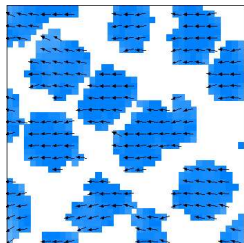
Figure 6: Dependence of the coercivity on the thickness for an iron-based negative nanonetwork.



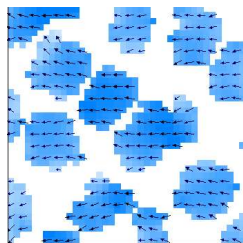
(a) Hysteresis curves for Ni nanowires



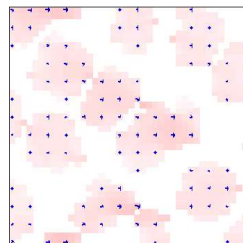
(b) Energy distributions



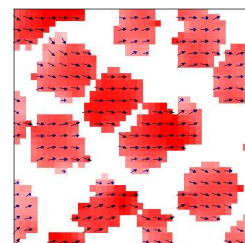
(c) Applied field -450 mT



(d) Applied field -360 mT



(e) Applied field 90 mT



(f) Applied field +180 mT

Figure 7: Overview of the dependence of the magnetic properties of nickel nanowires grown inside the NCA pores.

4.2 Magnetic properties of nickel nanowires as a function of the NCA pores

The simulation of the magnetic properties was performed on three types of Ni nanowire arrays grown inside pores of NCA templates with nominal pore sizes of 200, 100 and 20 nm. Various lengths of wires were analysed with the magnetic field applied parallel or perpendicular to the wire axis direction to obtain the hysteresis loops. Various geometrical resolutions (discretization level) were chosen as a function of the volume of the sample and length of the nanowires. To generate the hysteresis curve, a simulated external magnetic field was applied in a number of steps (50-60) with step size varying as a function of the field value.

The input parameters used for simulations are shown in the Table 1:

Parameter	Value
Anisotropy Constant, K_1	-4.5 kJ m^{-3}
Crystal planes	[111]/[200]
Exchange coefficient, A_x	24.5 pJ m^{-1}
Damping constant, α	0.5
Wire lengths range	10 to $48 \mu\text{m}$
Applied field	-450 to +450 mT

Table 1: Input parameters.

The parameters chosen in the simulations were conditioned to match experimental measurements. One of the simulations for the Ni nanowires grown inside the NCA pores included a wire length of 48 μm and the external magnetization field applied perpendicular to the wire axis direction is shown in Figure 7. The simulated hysteresis curve and corresponding experimental results are shown in Figure 7(a). Some of the energy distributions of the sample as a function of the applied magnetic field are presented in the Figure 7(b). Finally, the magnetisation maps in the plane perpendicular to the wire axis direction are shown in Figures 7(c) to 7(f). These results are typical of those obtained for various Ni nanowire configurations. All the results have been compared with experimental values to obtain statistical information regarding the effect of geometry on the properties of the Ni nanowires.

4.3 Effects of filling of the pores by magnetic material in the negative nanonetworks

It is very well known that during the generation of a negative nanonetwork by the sputtering method, the magnetic material is deposited not only on the NCA surface but also on the pores resulting in partial pore fill-ins. If the process of deposition continues, at a certain point all the pores become completely covered and a continuous film of magnetic material forms [3].

We have studied the effect of filling and its effects on the magnetic properties for a negative nanonetwork. In Figure 8, a simplified scheme of the cross section of a nanonetwork is depicted.

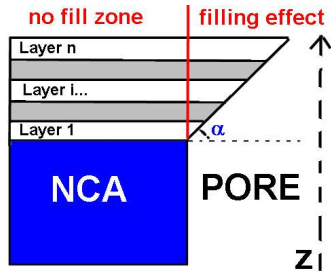


Figure 8: Cross-section for a nanonetwork.

The nanonetwork was divided into n layers and the filling effect was defined by the angle α . In an ideal case, where the filling effect is not present, α would correspond to an angle of 90 degrees.

The simulation study was performed for two cases:

- $\alpha=90^\circ$ that corresponds to the ideal case when *Layer 1* and *Layer n* have diameters of 100 nm.
- $\alpha=53^\circ$ that corresponds to a filling effect where the pore diameter is 100 nm and 70 nm for *Layer 1* and *Layer n*, respectively.

Simulations were performed for several configurations of a cobalt-based negative nanonetwork with the input parameters as shown in the following table:

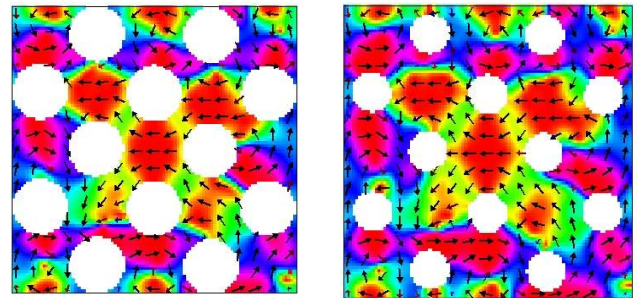
Parameter	Value
Pore/Interpore size	100 nm / 100 nm
Sample size	500 x 500 x 20 nm ³
Discretization cell	5 nm ³
Thickness/layers	20 nm / 5 layers
Uniaxial Anisotropy, K_l	520 kJ m ⁻³
Crystal plane	[0 0 1]
Exchange coefficient, A_x	30 pJ m ⁻¹
Damping constant, α	0.5
M_s	1425 kA m ⁻¹
Discretization cell	5 nm ³
Applied field	-1000 to +1000 mT

Table 2: Input parameters

The hysteresis curves are traced by applying a magnetic field along the surface of the nanonetwork (along the x axis) in a number of steps between maximum and minimum values (see Table 2).

Figures 9(a) and 9(b) show the distribution of magnetization in the x - y plane for *Layer 1* (bottom part of the nanonetwork) and *Layer n* (top part of the nanonetwork) for an applied magnetic field of 100 mT.

Here it can be noticed that with gradual pore filling, the distance between the pores grows with the decrease in the pore diameter on the top. The interaction between the magnetic regions in the top therefore, increases with respect to the bottom regions. This affects the magnetic properties of the nanonetwork.



(a) *Layer 1* for B =100 mT

(b) *Layer n* for B=100 mT

Figure 9: Magnetisation distributions in the x - y plane for a Co-based negative nanonetwork.

The energy distribution as a function of the applied field is presented in Figure 10. It clearly demonstrates the domination of the anisotropy energy.

A comparison between the anisotropy energies for the cases with $\alpha=90^\circ$ and $\alpha=53^\circ$ is shown in Figure 11. Here, a 2-3% variation in the amplitudes is noticed.

By calculating the coercivity values from the hysteresis curves, a decrease of 3% in the coercivity values was observed when the filling effect was included in the calculations.

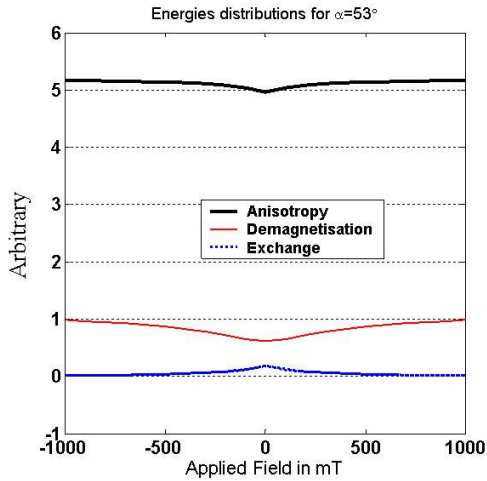


Figure 10: Energies distributions for the case with $\alpha=53^\circ$.

Theoretical predictions of coercivity variation were in accordance with the estimations given by the empirical relation given in the reference [3].

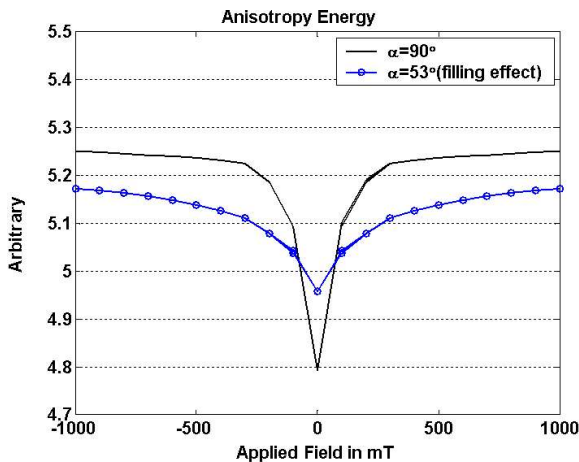


Figure 11: Anisotropy energy distributions.

5 CONCLUSIONS

In this paper, we have presented some of our results obtained from micromagnetic modelling of patterned nanostructured media. It was further shown that the capabilities of the codes are adequate in describing a large class of material configurations. Further studies for improving the resolution for a better approximation of the real geometries and various energy distributions that act in the magnetic dynamics are necessary. Nevertheless, it is very important to note that improvements should be correlated to the experimental data. This type of simulation can provide answer to the question of finding the best material for practical application such as future

recording devices. The simulation results show that not only the intrinsic physical properties of a certain material but the geometry also play an important role in determining the coercivity of the final media. Nickel has a low coercivity and consequently, combined with a not very high demagnetising field, seems to be a better choice for use as a soft magnetic nano device for providing medium range magnetic induction. Iron is also a good candidate for this purpose but has very high chemical reactivity and is easy to oxidise and therefore needs special precautions in realising nanostructures. Alloying with other elements such as Ni can solve this problem and will also provide a high magnetic induction. For perpendicular recording, that will allow the highest areal density of recording, a high coercivity media is required. Cobalt based structures are the most suitable for this purpose. The technical problems still remain to be solved for fabricating a recording head with a diameter less than 100 nm in order to be able read and write information bits in perpendicular recording mode by using cobalt cells.

6 Acknowledgements

This project is funded by a Fifth Framework Programme Marie Curie Host Development Fellowship award. The authors would like to thank K. M. Razeeb and S. A. M. Tofail for providing some of the experimental results.

7 REFERENCES

- [1] S. A. M. Tofail, I. Z. Rahman, and M. A. Rahman, "Patterned Nanostructured Arrays for High Density Magnetic Recording", *Applied Organometallic Chemistry*, 15 (5), 373-382 (2001)
- [2] J. Sellmyer, M. Zheng, and R. Skomski, "Magnetic properties of self-assembled Co nanowires of varying length and diameter", *J. Appl. Physics*, 87, 4718-4720 (2000)
- [3] S. A. M. Tofail, I. Z. Rahman, M. A. Rahman, R. Mahmood "Influence of nanoporosity and roughness on the thickness-dependent coercivity of iron nano-networks", *Chemical Monthly*, 133, pp. 859-872 (2002)
- [4] J. Sellmyer, M. Zheng, and R. Skomski, "Magnetism of Fe, Co and Ni nanowires in self-assembled arrays", *J. Phys. Condens. Matter.*, 13, pp. 433-460 (2001)
- [5] T. L. Gilbert, "A Lagrangian Formulation of the Gyromagnetic Equation of the magnetization Field", *Phys. Rev.*, Vol. 100, 1243 (1955)
- [6] M. J. Donahue and D. G. Porter, "NISTIR 6376", *NIST, Gaithersburg, MD* (1999)
- [7] R. D. McMichael and M. J. Donahue, "Head to head domain wall structures in thin magnetic strips", *IEEE Trans. Mag.* Vol. 33, 4167-4169 (1997)
- [8] E. Della Torre, "Fine particle micromagnetics", *IEEE Trans. Magn.* Vol. 21, pp. 1423-1425 (1985)
- [9] T. D. Leonhardt, R. J. M. van de Veerdonk, P. A. A. van der Heijden, T. W. Clinton, T. M. Crawford "Comparison of Perpendicular and Longitudinal Magnetic Recording Using a Contact Write/Read Tester", *IEEE Trans. Magn.*, 37, pp. 1580-1582 (2001)

[10] I. Z. Rahman, K. M. Razeed, M. A. Rahman, Md. Kamruzzaman, "Fabrication and characterization of

nickel nanowires deposited on metal substrate", *J. Magnetism and Mag.Mat.* 262,166-16 (2003)